Structural growth sequences and electronic properties of manganese-doped germanium clusters: $MnGe_n$ (2–15)

2008 J. Phys.: Condens. Matter 20 335223

(http://iopscience.iop.org/0953-8984/20/33/335223)

J. Phys.: Condens. Matter **20** (2008) 335223 (8pp) doi:10.1088/0953-8984/20/33/335223

Structural growth sequences and electronic properties of manganese-doped germanium clusters: $MnGe_n$ (2–15)

Jianguang Wang[1], Li Ma[1], Jijun Zhao[1,3] and Guanghou Wang[2]

[1] State Key Laboratory of Materials Modification by Laser, Electron, and Ion Beams, School of Physics, Optoelectronic Technology and College of Advanced Science and Technology, Dalian University of Technology, Dalian 116024, People's Republic of China
[2] National Laboratory of Solid State Microstructures, Nanjing University, Nanjing 210093, People's Republic of China

E-mail: zhaojj@dlut.edu.cn

Received 23 May 2008, in final form 11 July 2008
Published 31 July 2008
Online at stacks.iop.org/JPhysCM/20/335223

Abstract

The structural growth sequences and electronic properties of $MnGe_n$ ($n = 2$–15) clusters have been investigated using density functional theory (DFT) within the generalized gradient approximation (GGA). An extensive search of the lowest-energy structures was conducted by considering a number of structural isomers for each cluster size. In the ground-state structures of $MnGe_n$ clusters, the equilibrium site of the Mn atom gradually moves from the convex, surface to interior sites as the Ge cluster size varies from 2 to 15. The threshold size for the formation of caged $MnGe_n$ and the sealed Mn-encapsulated Ge_n structure is $n = 9$ and $n = 10$, respectively. Maximum peaks were observed for $MnGe_n$ clusters at $n = 3$, 6, 10, 12 and 14 with the size dependent on the second-order energy difference, implying that these clusters are relatively more stable. The electronic structures and magnetic properties of $MnGe_n$ in the ground-state structures are discussed. The doped Mn atom makes the HOMO–LUMO gap of the Ge_n clusters smaller, due to hybridization between the p states of the Ge atom and the d states of the Mn atom. Most of the Mn-doped Ge_n clusters carry a magnetic moment of about 1.0 μ_B, except that $MnGe_6$ and $MnGe_{11}$ have a magnetic moment of about 3.0 μ_B. Charge transfer between Mn and Ge was also observed.

(Some figures in this article are in colour only in the electronic version)

1. Introduction

Transition metal (TM)-doped silicon clusters are currently of great interest. The size selectivities, tunable gaps and magnetic properties of these clusters may lead to novel self-assembling semiconductor materials and new species for nanoscale applications. When different TM atoms are encapsulated into sufficiently large silicon cages, the hybrid system exhibits different behaviors regarding size selectivity, charge transfer and large highest occupied molecular orbital–lowest unoccupied molecular orbital (HOMO–LUMO) gaps [1–5]. Many investigations have focused on pure germanium clusters [6–14] or germanium clusters doped with halogen [15–17], Ni [18], Cu [19] or W [20]. With regard to TM-doped silicon clusters, much less effort has been devoted to metal-encapsulated germanium clusters, both theoretically and experimentally, until now [21–23]. Recent investigations on TM-doped germanium clusters indicate that they differ from TM-doped silicon clusters in their growth patterns [18]. Using *ab initio* pseudopotential planewave methods with the spin-polarized generalized gradient approximation, it was found that the growth behaviors of metal-encapsulated germanium clusters ($n = 14$–16) are different from those of metal-encapsulated silicon clusters. The large HOMO–LUMO gaps as well as the weak interaction between the host cluster and metal impurity make these species attractive for cluster-assembled materials. Using density functional theory,

[3] Author to whom any correspondence should be addressed.

Han *et al* [18–20] studied the growth patterns of TM-doped (TM = Ni, Cu and W) germanium clusters. They found that the critical size of the W-encapsulated germanium cluster structures is $n = 12$, while the remarkable fullerene-like W@Ge_n clusters emerge at $n = 14$, which are different from those of other TM dopants (Ni, Cu) with a critical size of $n = 10$ for the TM-encapsulated structures.

On the other hand, intentional doping of impurities into a host material is fundamental for controlling the functional properties, and is often a trigger for the emergence of novel physical phenomena. Interest in ferromagnetic (FM) semiconductors was rekindled with the discovery of spontaneous FM order in $In_{1-x}Mn_xAs$ [24] and $Ga_{1-x}Mn_xAs$ [25–27], when the FM properties were realized in semiconductor hosts already widely recognized for semiconductor device applications. These new FM semiconductor materials exhibit Curie temperatures up to 35 K and 110 K, respectively, for Mn concentrations of ∼5% and sufficiently high hole densities and have been closely studied for their potential in future spin-dependent semiconductor device technology. In addition to Mn:InAs and Mn:GaAs systems, the first ferromagnetic dilute magnetic semiconductor has been widely investigated recently [28–31]. Park *et al* [28] reported the epitaxial growth of a $Ge_{1-x}Mn_x$ ferromagnetic semiconductor with Curie temperature up to 116 K for $x = 0.033$.

Using first-principles density function theory (DFT), in this paper we report an extensive search for the lowest-energy configurations of $MnGe_n$ ($n = 2$–15) clusters by considering a considerable number of structural isomers. The size-dependent growth behavior and magnetic properties of the $MnGe_n$ clusters are discussed. The manganese atom was chosen as a dopant to investigate the effect of different sized Ge hosts on the magnetic moment of the TM impurity atom, which is related to the Mn_xGe_{1-x} dilute magnetic semiconductor with potential applications in semiconductor spintronics.

2. Theoretical methods

To search the lowest-energy structures of the $MnGe_n$ clusters we considered a large number of possible structural isomers for each size. For each cluster, a number of initial configurations were generated in three different ways: (1) substituting one Ge atom by Mn from the isomer structures of those Ge_{n+1} clusters [11]; (2) adopting from those known structures for TM-doped silicon clusters like $FeSi_n$ [32]; (3) hand-made construction following chemical intuition. The number of initial structural depends on the size of the cluster. For example, 13 initial configurations were considered for $MnGe_7$, while for the number of structural isomers increases to 20 for $MnGe_{12}$. After the initial structural isomers were constructed, full geometric optimizations were performed using spin-polarized DFT implemented in a DMol package [33]. All electron treatment and the double numerical basis set including the d-polarization function (DND) [33] were chosen. The exchange–correlation interaction was treated within the generalized gradient approximation (GGA) with the Perdew–Burke–Enzerhof (PBE) parameterization [34]. Self-consistent field calculations were done with a convergence criterion of 10^{-6} Hartree on the total energy. All the structures were fully optimized without any symmetry constraint with a convergence criterion of 0.002 Hartee $Å^{-1}$ for the forces and 0.005 Å for the displacement. Spin-unrestricted calculations were performed for all allowable spin multiplicities of the $MnGe_n$ clusters to reveal the possible magnetism of the clusters. The on-site charge and magnetic moment were obtained by Mulliken population analysis [35].

Table 1. Calculated results for $MnGe_n$ ($n = 2$–15) clusters, including the symmetry, the binding energy per atom (BE), the vertical ionization potential (VIP), the HOMO–LUMO gap, the on-site charge and spin moment (μ_s) of Mn atom, and the total spin moment (μ_{tot}) of $MnGe_n$ clusters for the lowest-energy structures.

Cluster	Symmetry	BE (eV)	VIP (eV)	Gap (eV)	Charge (e)	μ_s (μ_B)	μ_{tot} (μ_B)
$MnGe_2$	C_{2v}	2.041	7.343	0.378	0.030	2.322	1.000
$MnGe_3$	C_{3v}	2.549	6.786	0.687	0.100	2.408	0.999
$MnGe_4$	C_s	2.785	7.081	0.833	0.174	2.443	1.002
$MnGe_5$	C_{4v}	3.015	6.953	0.457	0.199	2.694	1.211
$MnGe_6$	C_{5v}	3.188	7.319	1.107	0.142	4.004	3.001
$MnGe_7$	C_{3v}	3.365	6.665	1.005	0.244	3.577	1.128
$MnGe_8$	C_{2v}	3.295	6.771	0.238	0.223	2.298	1.002
$MnGe_9$	C_{3v}	3.407	6.667	0.576	0.226	1.600	0.999
$MnGe_{10}$	C_s	3.476	6.424	0.313	0.293	2.339	1.002
$MnGe_{11}$	C_5	3.491	6.743	0.875	0.266	2.781	2.987
$MnGe_{12}$	I_h	3.591	6.892	1.178	0.252	2.007	1.001
$MnGe_{13}$	C_s	3.537	6.592	0.648	0.330	1.860	0.999
$MnGe_{14}$	C_{2v}	3.551	6.437	0.741	0.357	1.958	0.994
$MnGe_{15}$	C_1	3.477	6.283	0.691	0.345	1.976	1.001

3. Results and discussion

Using the computational scheme described above, we have optimized a number of low-lying isomers and determined the lowest-energy structures of $MnGe_n$ clusters up to $n = 15$. The obtained ground-state structures and some important low-lying metastable isomers are displayed in figures 1 and 2. The low-energy structures of pristine Ge_n clusters previously reported by our own group [11] are also plotted in figures 1 and 2 for comparison. The main calculated results, including symmetry, binding energy per atom, vertical ionization potential, HOMO–LUMO gap, on-site charge and spin moment of the Mn atom, and total spin moment for the lowest-energy structures of $MnGe_n$ clusters are listed in table 1.

3.1. Growth patterns of $MnGe_n$ ($n = 2$–8)

For the smallest clusters with $n \leqslant 4$, the pure Ge_n clusters adopt planar structures as their lowest-energy geometries [11]. The possible $MnGe_2$ geometries such as two linear isomers and a triangular structure are considered. The C_{2v} $MnGe_2$ (figures 1 and 2(a)) structure with the Mn atom directly attached to Ge_2 is optimized to be the most stable structure with two Mn–Ge bonds of 2.27 Å and one Ge–Ge bond of 2.60 Å. For the $MnGe_3$ clusters, the dominant geometries are planar and pyramidal structures. The ground-state pyramid

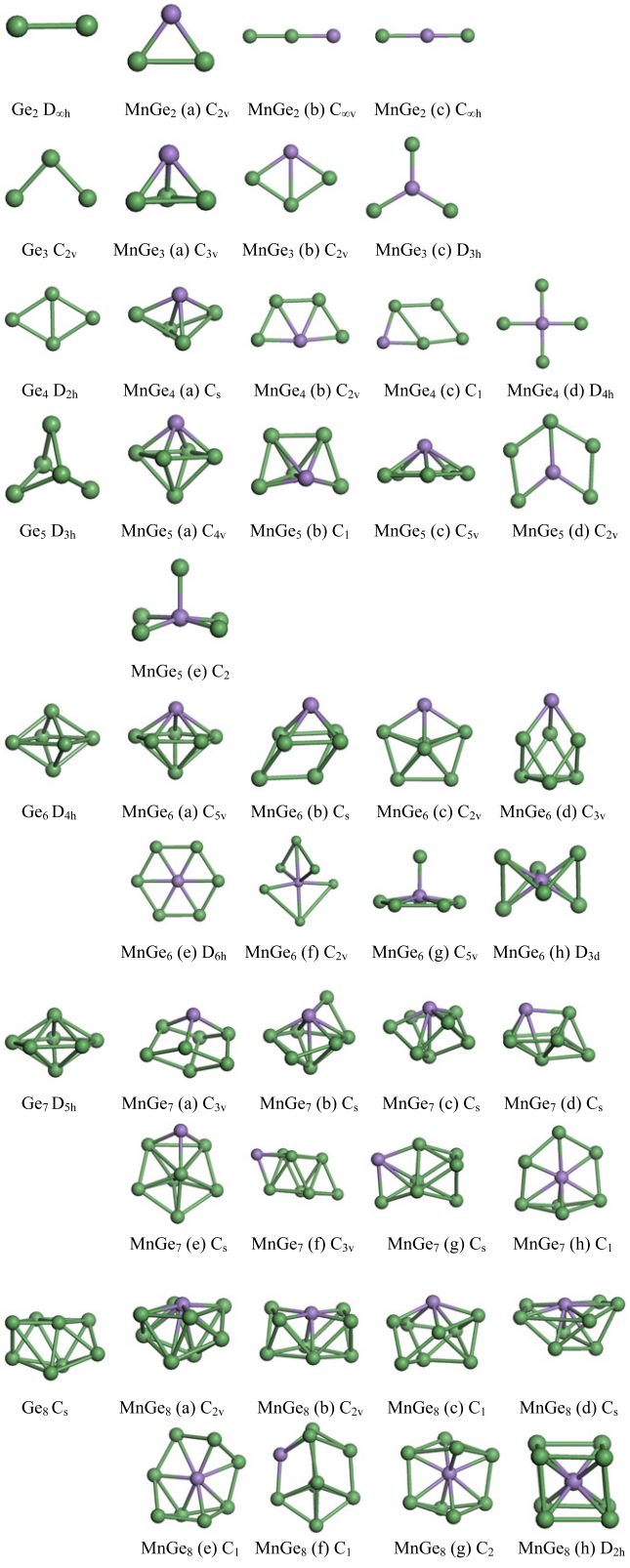

Figure 1. (Color online) Ground-state configurations and low-lying isomers of $MnGe_n$ ($n = 2$–8) clusters and the lowest-energy structures of pure Ge_n ($n = 2$–8) clusters. The first $MnGe_n$ structure is the lowest-energy one for $MnGe_n$ ($n = 2$–8). Green ball, germanium atoms; pink ball, manganese atoms.

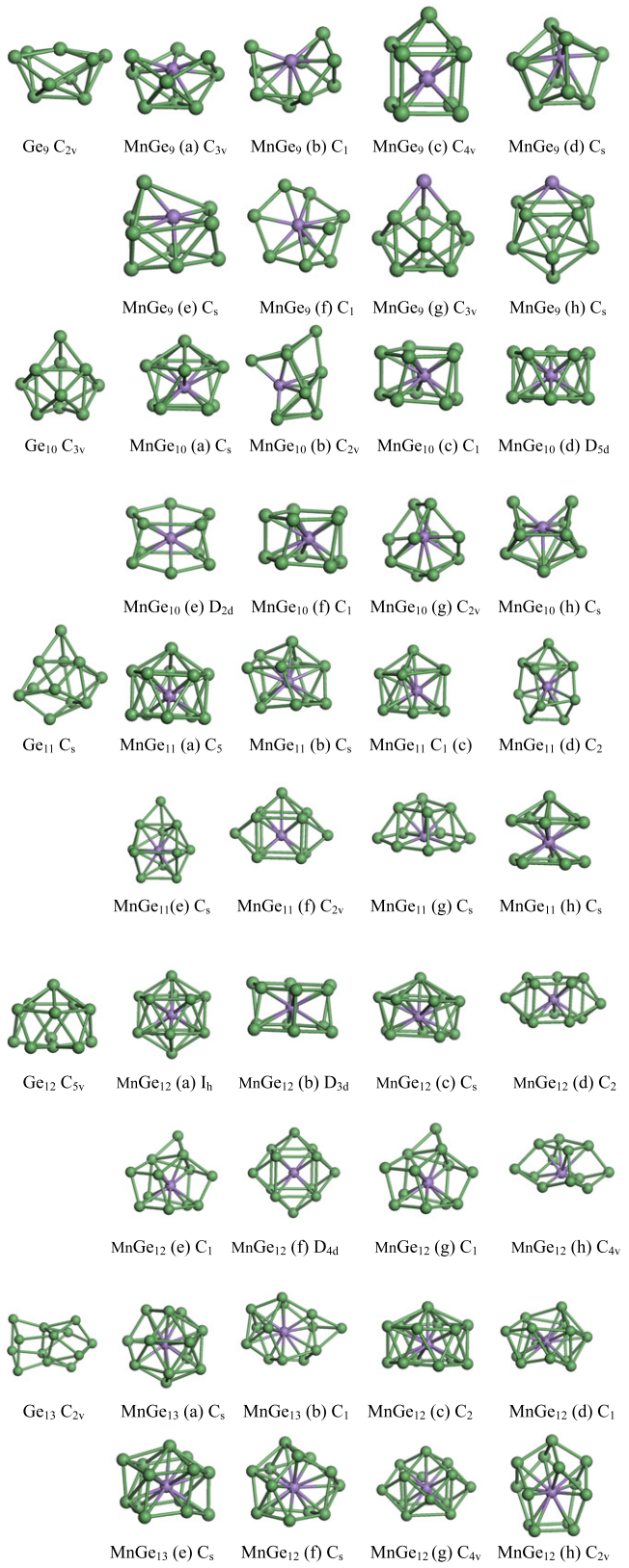

Figure 2. (Color online) Ground-state configurations and low-lying isomers of $MnGe_n$ ($n = 9$–15) clusters and the lowest-energy structures of pure Ge_n ($n = 9$–15) clusters. The first $MnGe_n$ structure is the lowest-energy one for $MnGe_n$ ($n = 9$–15). Green ball, germanium atoms; pink ball, manganese atoms.

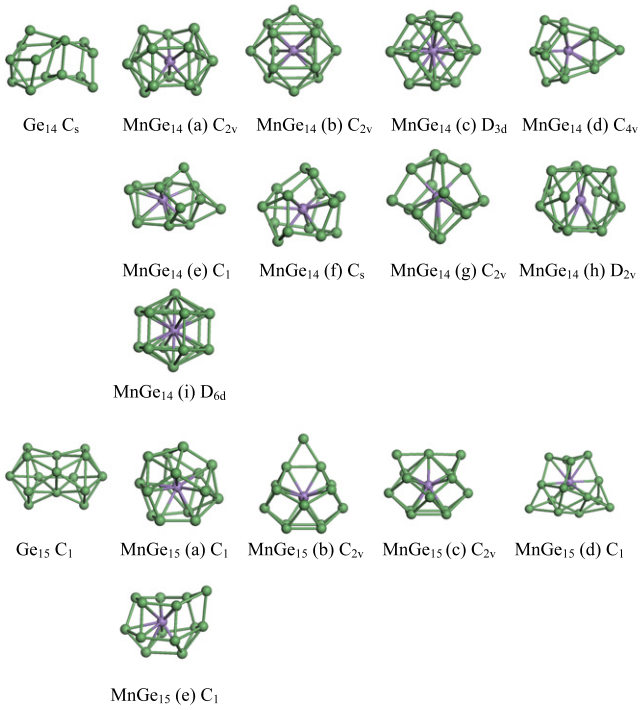

Figure 2. (Continued.)

structure of $MnGe_3$ (figures 1 and 3(a) C_{3v}) is lower in total energy than the planar rhombic 3b structure by 0.384 eV. The interactions between Mn and Ge atoms in the pyramidal structure are obviously stronger because that the Mn–Ge bond length (2.33 Å) in the pyramidal 3a structure is much shorter than that (2.98 Å) in the rhombic 3b (C_{2v}) structure. In the case of $n = 4$, the pure Ge_4 adopts a rhombic structure with D_{2h} symmetry. When Mn is edge-capped on two Ge atoms of the Ge_4 rhombus, the planar rhombus Ge_4 frame is distorted into the bent rhombus Ge_4 (C_s) (figures 1 and 4(a)). This structure has three Mn–Ge bonds of 2.36 Å and one Mn–Ge bond of 2.89 Å, which is lower in total energy than the Mn-centered trapezia (C_{2v}) by 0.449 eV; consequently, the C_s isomer is the most stable one found here.

As cluster size increases, the ground states for both Ge_n and $MnGe_n$ with $n \geqslant 5$ tend to adopt three-dimensional (3D) configurations. Guided by the ground-state configuration of $MnGe_4$, the analogous capped pattern is adopted for $MnGe_5$. On the basis of the bicapped quadrilateral Ge_6 (D_{4h}), the most stable structure for $MnGe_5$ with C_{4v} symmetry (5(a) in figure 1) can be formed when one top Ge atom in bicapped quadrilateral Ge_6 is substituted by one Mn atom. All the other structural isomers considered are energetically unfavorable, with an energy difference of more than 0.21 eV from the ground state.

As for the $MnGe_6$ cluster, based on the bicapped pentagonal Ge_7 (D_{5h}) cluster, the lowest-energy structure 6(a) with C_{5v} symmetry can be obtained when one Ge atom is substituted by one Mn atom. Similarly, the low-lying isomer 6(b) with C_s symmetry is obtained. The former one is lower in energy by 0.106 eV. Other isomers were obtained; however, their energies are higher than the most stable structure 6(a).

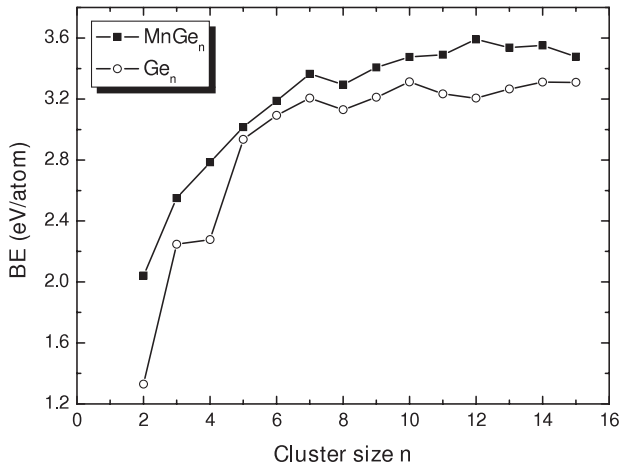

Figure 3. Size dependence of the binding energy per atom (BE) for the lowest-energy of $MnGe_n$ and Ge_n clusters.

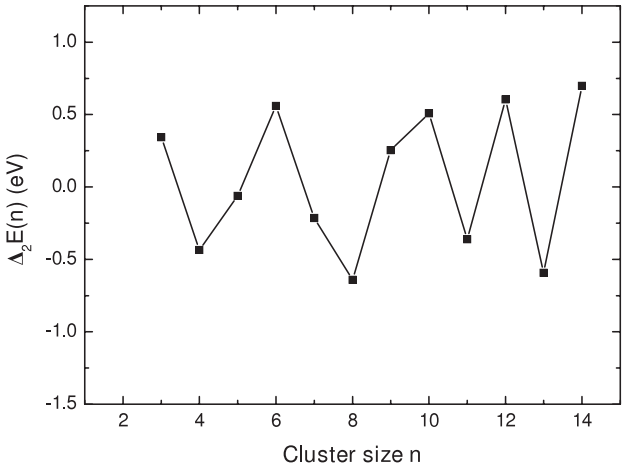

Figure 4. The second differences of $MnGe_n$ cluster energies for the lowest-energy structures $\Delta_2 E(n)$ as a function of the cluster size n.

The lowest-energy structure obtained for Ge_7 is a pentagonal bipyramid with D_{5h} symmetry. The ground-state structure obtained for $MnGe_7$ is a distorted cube with C_{3v} symmetry (7(a) in figure 1). Most structural isomers of $MnGe_7$ are displayed in figure 1; the Mn atoms locate at the vertex sites.

In the case of $MnGe_8$, a cage-like configuration with a surface Mn atom (C_{2v}) was obtained as the lowest-energy structure for $MnGe_8$ (8(a) in figure 1). This structure can be achieved by substituting the top Ge atom in a bicapped pentagonal bipyramid Ge_9 (C_s) by one Mn atom. The Mn-centered cubic structure with D_{2h} symmetry (8(h) in figure 1) was considered, but its energy is higher than the ground state by 1.176 eV. Several other isomers were considered; for example, Mn atoms locate on the surface of the cage-like structures for isomers 8b–8d, while Mn atoms move to the interior of the structures for isomers 8e–8h.

3.2. Growth patterns of $MnGe_n$ ($n = 9-15$)

Starting from the $MnGe_9$ cluster, an obvious divergence of growth behaviors between small-sized $MnGe_n$ clusters and

medium- or large-sized $MnGe_n$ clusters appears. For the $MnGe_9$ cluster, all isomers have cage-like configurations and Mn atoms gradually move into the interior sites. The lowest-energy structure of $MnGe_9$ (C_{3v}) (9(a) in figure 1) can be described as the convex Ge atom in the teracapped trigonal prism Ge_{10} (C_{3v}) being substituted by one Mn atom. However, the Mn atom is located in the interior of $MnGe_9$. In all other low-lying isomers, the Mn atoms locate in the interior of the structures.

As for the $MnGe_{10}$ isomers, the Mn atom has completely fallen into the germanium frame. Indeed, the Mn-encapsulated Ge_{10} structures are found to be dominant at such a cluster size. Similar to the multi-rhombic $NiGe_{10}$ [18] and $CuGe_{10}$ [19], the multi-rhombic concave $MnGe_{10}$ with C_s symmetry (10(a) in figure 1) is the most stable structure. Except for the stable concave 10(a), we also obtained a Mn-centered anti-pentagonal prism with D_{5h} symmetry (10(d) in figure 1) as the low-lying structure; however, its total energy is higher than that of the 10(a) isomer by 0.227 eV. On the basis of the optimized geometries, we should point out that the Mn-encapsulated structure 10(a) is different from the $TMSi_{10}$ clusters [36], while the structure of $MnGe_{10}$ is Mn-encapsulated Ge_{10} with C_s symmetry and the $TMSi_{10}$ is a TM-centered pentagonal prism with D_{5h} symmetry.

The lowest-energy structure of $MnGe_{11}$ (11(a) in figure 1) with C_5 symmetry can be obtained by capping one Ge atom on top of the Mn-centered pentagonal anti-prism of isomer 10(d). The metastable isomer 11(b) (C_s) has a similar type of configuration; however, its anti-pentagonal prism has become distorted. Previously, the $TMSi_{11}$ isomer was optimized using DFT calculations [32]. It was found that one Si atom capped on the top of a TM-centered pentagonal prism is the lowest-energy structure for $TMSi_{11}$.

For $n = 12$, a perfect Mn-centered icosahedron (I_h) 12(a) is found to be the lowest-energy structure for $MnGe_{12}$, whose energy is slightly lower than the distorted hexagonal prism (D_{3d}) (12(b) in figure 1) by 0.016 eV, in agreement with the previous calculation [36]. A distorted pentagonal-like prism with a Ge atom on the top (12(c) in figure 1, C_s symmetry) was found as the low-lying isomer with $\Delta = 0.215$ eV, which can be viewed as a continuation of the structure pattern of the lowest-energy structure of $MnGe_{11}$. The lowest-energy structure of $MnGe_{12}$ with a Mn-centered icosahedral (I_h) structure is different from that of the $TMSi_{12}$ clusters [32] with a TM-centered pentagonal prism with D_{5h} symmetry.

The most stable isomer for $MnGe_{13}$ 13(a) is cage-like with C_s symmetry, which is composed of six pentagons and one triangle. In the six pentagons, there are four pentagons capped with four Ge atoms on top of them. A low-lying 13(b) isomer, obtained from distorted pure Ge_{13} via Mn encapsulation, is found to be metastable, and its total energy is higher than that of the 13(a) isomer by 0.214 eV. A distorted pentagonal anti-prism with one Ge atom on the top (C_2) is obtained as another metastable isomer for $MnGe_{13}$ (13(c)), its energy is also higher than that of the 13(a) isomer.

The most stable structure of $MnGe_{14}$ 14(a) is achieved by a distorted pentagonal prism with top and edge-capping (C_{2v}). Two low-lying structures that are very close in energy were found for $MnGe_{14}$, one with C_{2v} symmetry 14(b), another with D_{3d} symmetry 14(c). For both structures, the Mn atoms sit at the center of the cages. The former one is lower in energy by 0.026 eV. All other isomers are higher than the lowest-energy structure by at least 0.531 eV in energy.

Among all candidate structures considered for $MnGe_{15}$, the most stable isomer (15(a)) with C_1 symmetry exhibits a cage-like Ge framework. Its energy is lower than those of the pyramidal (C_{2v}) (15(b)) or basket-like (C_{2v}) (15(c)) structures by 0.313 eV and 0.866 eV, respectively. Another basket-like isomer (15(d)) is obtained, but its symmetry has degenerated to C_1 and its total energy is higher than those of other isomers.

Compared with pure Ge_n clusters, doping with Mn atoms leads to substantial structural reconstruction. Generally speaking, the Mn atom in the lowest-energy configuration gradually moves from convex, to surface, and to the interior site as the size of the Ge_n cluster varies from $n = 2$ to 15. Starting from $n = 10$, the Mn in the $MnGe_{10}$ clusters completely falls into the center of the Ge frame and forms a cage. Similar behavior was observed in other $TMGe_n$ (TM = Ni, Cu and W) [18–20] clusters, while the cage-like structures form at $n = 7$ for $NiGe_n$, $n = 8$ for $CuGe_n$ and $n = 10$ for WGe_n. Such differences in the critical sizes for the formation of the Ge cage can be understood by the radius of the metal atom. Since a W atom is bigger than Mn, while Ni and Cu atoms are smaller than the Mn atom, more Ge atoms are needed to completely encapsulate the bigger transition metal atom. These findings further confirm that the metal-doped germanium clusters favor formation of endohedral cage-like structures and the lowest-energy configurations depend on the size of the metal atom and the number of Ge atoms.

3.3. Electronic and magnetic properties

In figures 3–9, the binding energy per atom, the second-order energy difference, the vertical ionization potential (VIP), the HOMO–LUMO gaps, the partial density of states of some $MnGe_n$ clusters, the HOMO–LUMO orbitals of some Mn atom centered cage-like structures for $n = 10$–15 clusters, and the atomic spin moment and atomic charge of the Mn atom are depicted, respectively. The binding energy of pure Ge_n ($n = 2$–15) clusters is also plotted in figure 3 for comparison. It can be seen that the binding energy per atom of $MnGe_n$ ($n = 2$–15) clusters is usually larger than that of pure Ge_n clusters. Thus, doping with Mn atoms improves the stability of pure Ge_n clusters.

In cluster physics, the second-order difference of cluster energies, $\Delta_2 E(n) = E(n+1)+E(n-1)-2E(n)$, is a sensitive quantity that reflects the relative stability of clusters [11]. Figure 4 shows the second-order difference of cluster total energies, $\Delta_2 E(n)$, as a function of cluster size. Local peaks are found at $n = 3$, 6, 10, 12 and 14, which indicates that these five clusters are relatively more stable than their neighbors. However, there is no very pronounced peak among the observed maxima, indicating that none of these clusters is particularly stable.

The size dependence of VIP is also calculated and plotted in figure 5. $MnGe_6$ possesses the largest vertical ionization

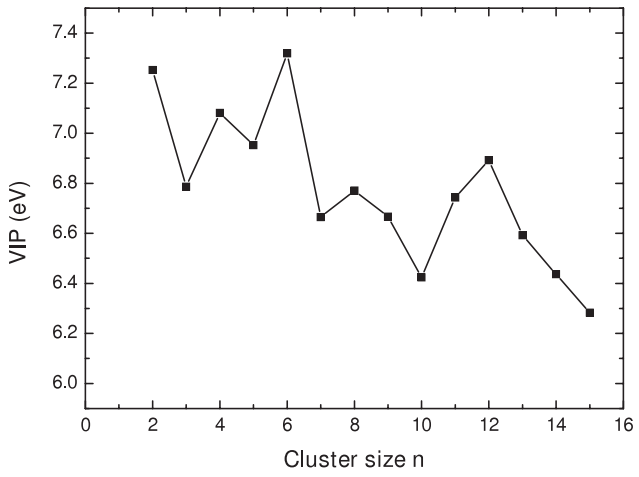

Figure 5. Size dependence of the vertical ionization potential VIP for the lowest-energy of $MnGe_n$ clusters.

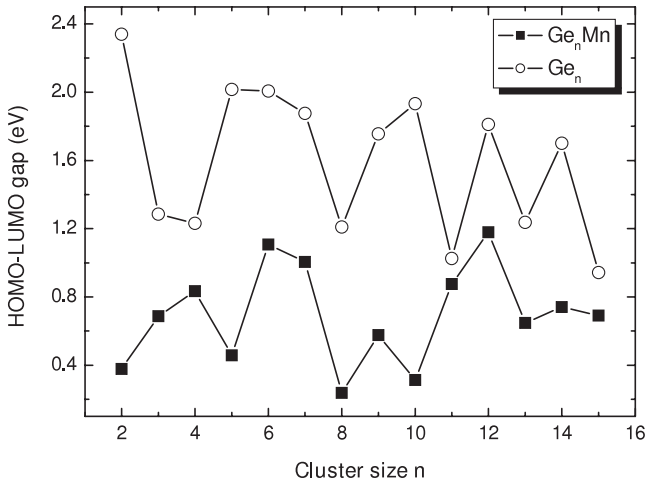

Figure 6. Size dependence of the HOMO–LUMO gaps of the lowest-energy for $MnGe_n$ and Ge_n clusters.

potential, corresponding to its higher stability. Han *et al* found that $NiGe_{10}$, WGe_8 and $CuGe_{10}$ are more stable than their neighbors [18–20]. The difference can be interpreted by factors such as the size of metal atom and the geometric structure. For example, the closed-cage configuration of icosahedron $MnGe_{12}$ might contribute to the higher stability of the Mn-doped clusters.

The size dependence of HOMO–LUMO gaps for $MnGe_n$ ($n = 2$–15) and Ge_n ($n = 2$–15) clusters is plotted in figure 6. It can be seen that doping with Mn atoms induces less oscillation of the HOMO–LUMO gap than in pure Ge_n clusters. Thus, mixed clusters exhibit a more metal-like character upon Mn doping. In order to further understand the effect of the HOMO–LUMO gap, we have performed detailed analysis of the molecular orbitals by examining the partial density of states from the contribution of different orbitals components (s, p, d) and the electron density of the HOMO–LUMO states. Figure 7 gives the partial density of states (PDOS) of some representative $MnGe_n$ clusters ($MnGe_6$, $MnGe_{10}$, $MnGe_{12}$ and $MnGe_{15}$). It can be clearly seen that the electronic states in the vicinity of the Fermi level mainly come from p and d states and the contribution from the s state is very small. Similar behavior was observed for all the other sized clusters. The electron densities of the HOMO and LUMO states of the $MnGe_n$ ($n = 10$–15) clusters with Mn-centered cage-like configurations are shown in figure 8. Both the HOMO and LUMO states are mainly localized around the Mn atom, while there is also some electron distribution around the Ge atoms. Figures 7 and 8 together indicate that the HOMO and LUMO are composed of the Mn d states mixed with Ge p states. Thus, the p–d hybridization should be responsible for the size-dependent behavior of the HOMO–LUMO gap. This effect may provide a valuable pathway for controlling the HOMO–LUMO gap by appropriately choosing a transition metal atom and doping it inside germanium clusters, similar to $TM@Si_n$ clusters [32, 37]. On the other hand, our spin-unrestricted calculations reveal that the HOMO and LUMO have the same spin states for most $MnGe_n$ clusters ($n = 3, 5, 6, 7, 8, 10, 11, 14$ and 15), namely, spin-up (majority) states. For the $MnGe_n$ clusters with $n = 2, 4, 9, 12$ and 13, the HOMO and LUMO correspond to different spin states, that is, the HOMO possess a spin-down state and the LUMO have a spin-up one at $n = 2$, 4 and 12, the HOMO possesses a spin-up state and the LUMO has a spin-down one at $n = 9$ and 13.

We have also examined the magnetic behavior of the TM atom inside the Ge clusters. In table 1, we summarize the local magnetic moments on the Mn atom and total magnetic moments of the Mn-doped Ge_n clusters, and the former are also plotted in figure 9(a). Interestingly, the total magnetic moment of the $MnGe_n$ clusters is not a monotonic function of cluster size. Most $MnGe_n$ clusters carry a total magnetic moment of about 1.0 μ_B, whereas the total spin moment of $MnGe_6$ and $MnGe_{11}$ reaches 3.0 μ_B. For the $MnGe_n$ ($n = 2$–15) clusters, the magnetic moment (about 2.0–4.0 μ_B) is mainly located on the Mn site. As shown in figure 9(a), the size dependence of magnetic moment for the Mn atom exhibits a three-step behavior. For the smallest clusters with $n = 2$–6, there is a relatively slow increase in magnetic moment, reaching a maximum at $n = 6$. Then, the spin moment of the Mn atom decreases from $n = 6$–10 and reaches a minimum at $n = 10$. From $n = 11$–15, the magnetic moment of the Mn atom remains almost constant ($\sim$2.0 μ_B). A small amount of spin was found on the Ge sites, while most of the local moments on Ge atoms were found to align antiferromagnetically with respect to that on the Mn atom.

To further understand the variation of the magnetic moment, the on-site charges of Mn atoms for the lowest-energy structures of the $MnGe_n$ ($n = 2$–15) clusters were performed by Mulliken population analysis, and are presented in figure 9(b). For all of the systems studied, the charge transfer occurs in the same direction, namely from the Ge atoms to the Mn atom. Overall, the size dependence of charge transfer for the $MnGe_n$ ($n = 2$–15) increases with increasing cluster size. As shown in figure 9, there is a correspondence between the charge transfer and the magnetic moment for the Mn atom. For example, the largest magnetic moment of the Mn atom in a $MnGe_6$ cluster is about 4.0 μ_B, while the amount of charge transferred on the Mn atom is relatively small, about

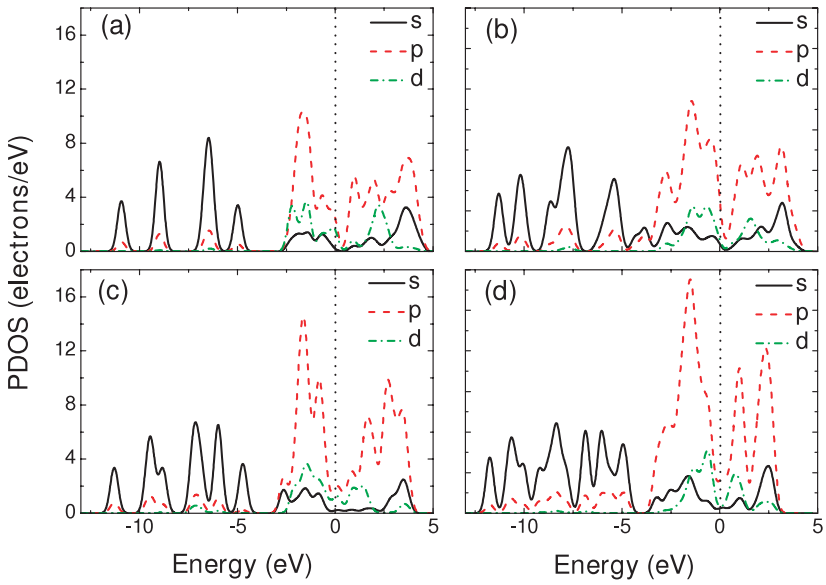

Figure 7. The partial density of states (PDOS) of s, p and d orbitals for (a) $MnGe_6$, (b) $MnGe_{10}$, (c) $MnGe_{12}$ and (d) $MnGe_{15}$. The vertical line indicates the Fermi level.

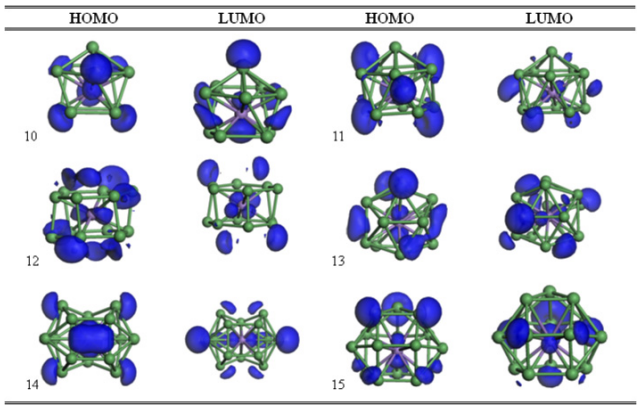

Figure 8. The HOMO and LUMO orbitals of the Mn-centered cage-like configurations for $n = 10$–15 clusters. The isovalue is 0.04.

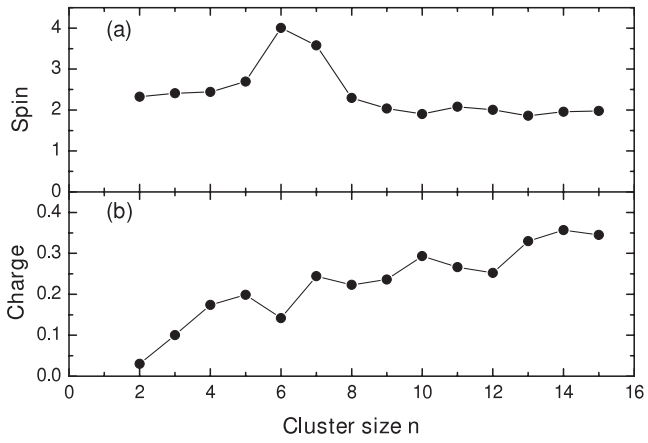

Figure 9. Size dependence of the on-site spin moment and charges of the Mn atom for the lowest energy for $MnGe_n$ clusters.

0.14 electrons. For the $MnGe_{10}$ cluster, the amount of charge transferred on the Mn atom is 0.29 electrons, while the rest of the magnetic moment for the Mn atom is about 1.9 μ_B. This result implies that charge transfer between Mn and Ge might partially account for reduction in the magnetic moment of the Mn atom. On the other hand, the transition size for formation of a Ge cage is around $n = 9$ and 10. Therefore, there might be some correlation between the geometric structure of the Ge framework and the magnetic moment of the encapsulated Mn atom.

4. Conclusion

The growth behavior, stability and electronic and magnetic properties of $MnGe_n$ ($n = 2$–15) clusters were investigated theoretically using DFT-GGA calculations. For each cluster size an extensive search of the lowest-energy structures was performed by considering a number of structural isomers. In the ground-state structures of $MnGe_n$ clusters, the equilibrium site of Mn atom gradually moves from convex, surface to interior sites as cluster size n increases from 2 to 15. The threshold size of the caged $MnGe_n$ and the critical size of the Mn-encapsulated Ge_n structure emerge at $n = 9$ and 10, respectively. According to the second-order energy difference, $MnGe_n$ clusters at $n = 3$, 6, 10, 12 and 14, possess relatively higher stability. The electronic structures and magnetic properties of these $MnGe_n$ in the ground-state structures were discussed. We find that the doped Mn atom makes the HOMO–LUMO gap of the pure Ge_n clusters smaller, due to hybridization between the p states of the Ge atom and the d states of the Mn atom. The HOMO and LUMO have spin-up (majority) states for most $MnGe_n$ clusters. The electron density of the HOMO and LUMO states of the cage-like $MnGe_n$ configurations mainly localize at the Mn atom.

Most ground-state structures of Mn-doped Ge_n clusters carry a magnetic moment of about 1.0 μ_B, except that $MnGe_6$ and $MnGe_{11}$ have a magnetic moment of about 3.0 μ_B. Charge transfer between Mn and Ge show some correspondence to the magnetic moment. The present theoretical results show that the electronic properties like the HOMO–LUMO gap and magnetic moment can be tuned by choosing an appropriate transition metal atom and doping it inside germanium clusters of particular sizes.

Acknowledgments

This work was supported by the NCET Program provided by the Ministry of Education of China (NCET06-0281), National Key Basic Research Development Program of China (no. 2007CB613902), the Chinese Postdoctoral Science Foundation (20060400289, 20070421052), the National Natural Science Foundation of China (90606002, 10774019), and the PhD Programs Foundation of the Education Ministry of China (20070141026).

References

[1] Beck S M 1987 *J. Chem. Phys.* **87** 4233
Beck S M 1989 *J. Chem. Phys.* **90** 6306
[2] Hiura H, Miyazaki T and Kanayama T 2001 *Phys. Rev. Lett.* **86** 1733
[3] Lu J and Nagase S 2003 *Phys. Rev. Lett.* **90** 115506
[4] Singh A K, Briere T M, Kumar V and Kawazoe Y 2003 *Phys. Rev. Lett.* **91** 146802
[5] Miyazaki T, Hiura H and Kanayama T 2003 *Eur. Phys. J.* D **24** 241
[6] Rata I, Shvartsburg A A, Horoi M, Frauenheim T, Siu K W M and Jackson K A 2000 *Phys. Rev. Lett.* **85** 546
[7] Mitas L, Grossman J C, Stich I and Tobik J 2000 *Phys. Rev. Lett.* **84** 1479
[8] Shvartsburg A A, Liu B, Liu Z Y, Wang C Z, Jarrold M F and Ho K M 1997 *Phys. Rev. Lett.* **83** 2176
Liu Z Y, Wang C Z and Ho K M 2000 *Phys. Rev.* B **61** 2329
[9] Wang J L, Zhao J J, Ding F, Shen W F, Lee H and Wang G H 2001 *Solid State Commun.* **117** 593
Wang J L, Zhao J J and Wang G H 2000 *Phys. Lett.* A **275** 281
[10] Han J G 2000 *Chem. Phys. Lett.* **324** 143
[11] Wang J L, Wang G H and Zhao J J 2001 *Phys. Rev.* B **64** 205411
[12] Archibong E F and St-Amant A 1998 *J. Chem. Phys.* **109** 962
[13] Ogut S and Chelikowsky J R 1997 *Phys. Rev.* B **55** 4914
[14] Li B X and Cao P L 2000 *Phys. Rev.* B **62** 15788
[15] Yoshida S and Fuke K 1999 *J. Chem. Phys.* **111** 3880
[16] Negishi Y, Kawamata H, Hayase T, Gomei T, Kishi R, Hayakawa F, Nakajima A and Kaya K 1997 *Chem. Phys. Lett.* **269** 199
[17] Kaya K, Kawamata H, Negishi Y, Hayase T, Kishi R and Nakajima A 1997 *Z. Phys.* D **40** 5
[18] Wang J and Han J G 2006 *J. Phys. Chem.* **110** 7820
[19] Wang J and Han J G 2005 *J. Chem. Phys.* **123** 244303
[20] Wang J and Han J G 2006 *J. Phys. Chem.* **110** 12670
[21] Zhang X, Li G and Gao Z 2001 *Rapid. Commun. Mass Spectrom.* **15** 1573
[22] Liu J and Nagase S 2003 *Chem. Phys. Lett.* **372** 394
[23] Goicochea J M and Sevov S C 2005 *J. Am. Chem. Soc.* **127** 7676
[24] Munekata H, Ohno H, von Molnar S, Segmüller A, Chang L L and Esaki L 1989 *Phys. Rev. Lett.* **63** 1849
[25] De Boeck J, Oesterholt R, Van Esch A, Bender H, Bruynseraede C, Van Hoof C and Borghs G 1996 *Appl. Phys. Lett.* **68** 2744
[26] Ohno H, Shen A, Matsukura F, Oiwa A, Endo A, Katsumoto S and Iye Y 1996 *Appl. Phys. Lett.* **69** 363
[27] Ohno H 1998 *Science* **281** 951
[28] Park Y D, Hanbicki A T, Erwin S C, Hellberg C S, Sullivan J M, Mattson J E, Ambrose T F, Wilson A, Spanos G and Jonker B T 2002 *Science* **295** 651
[29] Rareev R R, Bugoslavsky Yu V, Schreiber R, Paul A, Sperl M and Döppe M 2006 *Appl. Phys. Lett.* **88** 222508
[30] Jaeger C, Bihler C, Vallaitis T, Goennenwien S T B, Opel M, Gross R and Brandt M S 2006 *Phys. Rev.* B **74** 045330
[31] Arantes J T, Da Silva Antônio J R, Fazzio A and Antonelli A 2007 *Phys. Rev.* B **75** 075316
[32] Ma L, Zhao J J, Wang J G, Wang B L, Lu Q L and Wang G H 2006 *Phys. Rev.* B **73** 125439
[33] Delley B 1990 *J. Chem. Phys.* **92** 508
[34] Perdew J P, Burke K and Ernzerhof M 1996 *Phys. Rev. Lett.* **77** 3865
[35] Mulliken R S 1955 *J. Chem. Phys.* **23** 1841
[36] Singh A K, Kumar V and Kawazoe Y 2004 *Phys. Rev.* B **69** 233406
[37] Khanna S N, Rao B K and Jena P 2002 *Phys. Rev.* B **89** 016803